Results in Engineering 25 (2025) 103570

Contents lists available at ScienceDirect

Results in Engineering

journal homepage: www.sciencedirect.com/journal/results-in-engineering

Research paper

# Machine learning for predicting resistance spot weld quality in automotive manufacturing

Nuttapong Chuenmee [a], Nattachai Phothi [b], Kontorn Chamniprasart [a], Sorada Khaengkarn [a], Jiraphon Srisertpol [a,*]

[a] Mechatronics Engineering Program, School of Mechanical Engineering, Suranaree University of Technology, Nakhon Ratchasima, Thailand
[b] Department of Production Engineering Technology, Faculty of Industrial Technology, Loei Rajabhat University, Loei, Thailand

ARTICLE INFO

*Keywords:*
Resistance spot welding (RSW)
Weld inspection
Weld quality classification
Data analysis
Machine learning

ABSTRACT

Resistance Spot Welding (RSW) stands as the primary joining process in the automotive industry, renowned for its suitability for automation and integration into high-production assembly lines. Despite its advantages, accurately evaluating RSW remains challenging, resulting in additional costs and production steps. Current inspection methods, reliant on random checks after cars leave the Body-in-White (BIW), often lead to significant time losses, emphasizing the necessity for enhanced quality assessment. This study aims to transition from random checks to 100 percent inspection using data analysis and machine learning techniques. By predicting weld quality levels prior to car body completion, this approach aims to improve quality control. Five distinct algorithms—Artificial Neural Network (ANN), Convolution Neural Network (CNN), Long Short-Term Memory (LSTM), Random Forest Classifier (RFC), and Extreme Gradient Boosting (XGBoost)—were assessed. The research highlights that the proposed methodology, particularly leveraging XGBoost, achieves a notable prediction accuracy of 97.1% when applied to unseen data.

## 1. Introduction

In the assembly of automobile parts, quality control in welding is paramount, ensuring the durability and safety of the vehicle. Welding, which accounts for a quarter of the primary manufacturing processes in car manufacturing, demands strict adherence to quality and precision standards. According to the Federation of Thai Industries, Thailand's vehicle production from January to December 2023 nearly reached two million, with pickup trucks accounting for over 1.1 million units, or 62.7% of total production. A typical pickup truck consists of more than 15,000 essential components, including the engine, transmission, suspension, steering systems, brakes, wheels, interior features, electrical and safety systems, and the body and frame, which vary according to the model. The car body is the primary focus of welding operations, with the monocoque design being a common technique for constructing vehicle bodies, involving the assembly and welding of over a hundred steel parts to form the car's structure.

In the automotive body assembly industry, some components still necessitate human labor welding due to cost constraints, while industrial robots can weld nearly all components. An automotive assembly plant might have as many as 300 welding robots, and the plant we studied has been using welding robots for over seven years. Despite rigorous maintenance to preserve welding efficiency, the search for measuring instruments to assess welding quality remains a vital aspect of quality control. Instruments such as force sensors [1], distance sensors [2], vision camera [3], thermal cameras [4,5], vibration sensors [6] and acoustics sensors [7] are considered, though their high costs significantly impact production expenses, as each robot would need its own installation. This raises an important question: is this investment worthwhile?

Currently, the plant we studied employs a random sampling method for welding quality [8,9] checks, in line with IATF 16949:2016, utilizing Ultrasonic Testing (UT) [10], pry-bar testing [11], and teardown method [12]. Among these, UT is widely used despite its high cost, as it allows for post-welding inspections to measure material thickness and detect defects. However, UT inspections are limited by their random sampling approach and are conducted only after the monocoque body assembly is complete, potentially missing critical defects. Each inspection requires a team of 12 persons, including 1 engineer, 3 technicians, and 8 inspectors, underscoring the resource-intensive nature of the current system.

* Corresponding author.
*E-mail address:* jiraphon@sut.ac.th (J. Srisertpol).

https://doi.org/10.1016/j.rineng.2024.103570
Received 29 August 2024; Received in revised form 20 November 2024; Accepted 27 November 2024

Available online 20 December 2024

The efficient utilization of advanced manufacturing technologies, as shown in studies applying Finite Element Analysis (FEA) and response surface methods for design optimization [13], highlights the potential for system-wide improvements. In the existing automated systems, only 5% of weld joints are inspected, with heavy reliance on low-density manual inspections. With the integration of Machine Learning for Predicting Resistance Spot Weld Quality, inspection coverage has been enhanced to 100%. This transformative improvement significantly reduces dependency on manual labor while enabling targeted inspections in areas of concern, thereby improving efficiency and accuracy.

Currently, UT pry inspections are performed at a rate of one inspection per joint per shift. In newly launched systems, the machine learning framework aims to achieve 90%–95% inspection coverage for joints, with recurring inspections on stable joints expected to decrease from once per shift to once per week during the transitional phase. Additionally, the system provides real-time notifications for areas requiring attention, further augmenting the overall inspection process and driving proactive quality assurance.

A clear example of this impact is when a weld in the Floor Panel Carrier System fails to meet the factory's quality standards. The team then analyzes the cause and origin of the defect to determine the specific process in which it occurred. For instance, was the defect introduced during the welding of the Floor Panel Carrier System itself or during its assembly with other parts in the monocoque body construction? If the analysis indicates that the defect originated in the welding process of the Floor Panel Carrier System, the production line halts immediately to inspect all related parts, tracing back to the BIW. This rapid response is feasible because the defect's location on the part is precisely identified, and inspecting a single weld defect takes no more than two minutes. If additional parts with substandard welds are discovered during the inspection, they are gathered and sent for repair before being reintegrated into the production line. Although the defect was identified only in the Floor Panel Carrier System welds, the simultaneous welding of other parts in the monocoque body construction necessitates halting the entire production line. This halt affects multiple sections—including the Dash Compartment, Rear Compartment, Roof, Left-Side Frame, and Right-Side Frame (as illustrated in Fig. 5)—until the inspection and repair of the Floor Panel Carrier System welds are completed. The inspection process is thorough, covering more than just the welding procedure of the Floor Panel Carrier System. It includes a forward trace, in which previously assembled monocoque bodies are also inspected—reviewing 30 vehicles per inspection cycle, equivalent to approximately one hour of production. This forward trace continues until the Floor Panel Carrier System is confirmed to be free of weld defects within the cycle. If a defect is detected, an additional retrospective inspection is carried out, reviewing another 30 vehicles.

In 2022, when an incident report revealed that 120 out of 600 manufactured vehicle bodies exhibited weld quality issues at the BIW stage. This resulted in approximately 10 hours of inspection and repair time, equivalent to a full day of remedial work. Furthermore, one vehicle displayed performance issues after production, prompting the company to assemble a team of specialists for a thorough investigation. The analysis traced the problem to welds that did not meet required standards, identifying inferior weld seams as the primary cause. This led to a temporary suspension of the BIW process to allow the team to examine the welding robots and guns, implement corrective actions, and improve the process.

The examples provided demonstrate that the weld quality inspection process occurs after the completion of the monocoque body. If the welds do not meet the required standards, it is necessary to trace back to the BIW process and monocoque body simultaneously in both directions, resulting in considerable time and labor expenditures. This raises a critical question: is it possible to evaluate welding quality in real-time during welding robot operation, enabling immediate corrections before advancing to the monocoque body welding phase? This research aims to leverage Industry 4.0 technologies to transform the existing inspection process into an automated system [14–17]. By harnessing data from welding robots and incorporating artificial intelligence, we aim to identify and categorize weld quality, enhancing the efficiency and accuracy of the inspection process.

This research focuses on evaluating the weld quality of Front/Rear floor components in vehicles. These components are shaped from sheet metal through a pressing process and joined using Resistance Spot Welding (RSW) [18] to create a larger assembly known as the Floor Panel Carrier System. This assembly is integral to the vehicle's structure, providing the base of the passenger compartment and distributing stress and weight evenly. It also collaborates with other components to mitigate impact forces, safeguarding passengers. Typically, this welding is executed by automated robots. Ensuring the precision and quality of RSW is critical for the vehicle's safety and structural integrity. Nevertheless, accurately assessing RSW quality poses significant challenges.

The weld quality inspection process commonly identifies six defect types: undersized, discrepant, edge, missing, off-location, and explosion defects. This research focuses on three defect types: undersized, discrepant, and explosion. Undersized and discrepant defects are grouped under the term "Cold weld" in accordance with the factory's quality standards, as they pose safety risks and require repair before the components are sent to the paint shop. Explosion defects are included due to their high frequency and potential severity. This paper introduces an AI-enhanced inspection process that categorizes weld quality into three levels: Level 0 for "Satisfy," Level 1 for "Expulsion," and Level 2 for "Cold weld."

The aim is to create a real-time system for immediate detection of welding defects, ensuring complete inspection of every vehicle structure, thereby achieving 100% inspection coverage. This is a significant improvement over the current method, which randomly inspects only 5% of production using a combination of non-destructive and destructive tests. The proposed system is expected to attain a minimum accuracy rate of 90% to be considered effective.

## 2. Literature reviews

In a study by Sim and Yun Kim [19], the researchers propose a hybrid prediction method that combines a theoretical physical model with a machine learning approach. This hybrid method integrates the theoretical model with spline interpolation, establishing a mathematical framework for predicting nugget growth and formation in RSW. Experimental results indicate that the proposed hybrid method produces more accurate and meaningful predictions compared to existing algorithms when applied to RSW datasets. Furthermore, the hybrid method demonstrates robustness to data errors, making it a durable and reliable prediction approach.

Wang et al. [20] conducted a study utilizing a particle swarm optimization (PSO) algorithm for intelligent parameter measurement in a three-phase medium-frequency direct current (MFDC) RSW machine. To evaluate the accuracy and reliability of these measurements, a numerical model was developed using MATLAB Simulink. The comparative analysis indicated a maximum error of only 1% across all measured parameters, underscoring the effectiveness of the proposed intelligent parameter measurement method and demonstrating its ability to deliver accurate and reliable results for the RSW machine.

In their study, Yu et al. [21] introduced a reference-based adaptive RSW method aimed at mitigating the shunting effect in short-pitch ($\leq$40 mm) RSW. They developed an exponential model to predict weld pitch as a function of dynamic factors, analyzed the relationship between nugget diameter and heat input relative to weld pitch, and established a logistic growth model for predicting heat input compensation. Experimental results showed that this approach increased nugget diameter and decreased the shunting effect compared to conventional welding methods. These findings underscore the effectiveness of the proposed reference-based adaptive RSW method in minimizing the shunting effect in short-pitch RSW.

Dwibedi et al. [22] investigated the effects of weld time on joint strength, nugget size, and fracture mode in Hastelloy X weldments, a Nickel-Chromium-Iron-Molybdenum alloy, produced via the RSW process. The study aimed to determine the parameters and primary causes of failure using fractography, which analyzes the fracture surfaces of materials using Scanning Electron Microscopy (SEM). The principal findings indicated that the diameter of the weld nugget increased proportionally with weld time, and the joint strength of the spot-welded alloy improved until reaching an optimal weld duration. Nonetheless, the application of excessive heat and electrode pressure during the welding process initiated cracking.

Moshayedi and Sattari-Far [23] explored the correlation between nugget size, welding time, and current, comparing predicted nugget sizes with actual experimental results using a two-dimensional finite element model. This model, developed through fully coupled electrical-thermal and incrementally coupled thermal-mechanical analyses. The study also investigated variations in pressure and contact area during the welding process. Findings indicated compressive stress at the nugget center, with tensile stress increasing toward the edge. The highest tensile stress appeared outside the nugget, near its periphery. Additionally, radial residual stress magnitudes in the inner and outer areas of the weld nugget rose with increased welding time and current, though a slight decrease was observed in the edge regions of the nugget.

In their study, Podržaj et al. [24] developed an experimental setup to investigate the effects of poor fit-up conditions on welding outcomes. This setup enabled the measurement of welding force during the initial contact between electrode tips and weld pieces, considering varying intensities of deformation and pin distances. Additionally, the system allowed precise quantification of welding force during initial contact. To reduce the negative impact of poor fit-up conditions on weld strength, the researchers examined the introduction of a preheating phase. While preheating improved weld strength, a notable disparity remained between the weld strength of non-deformed welds and those under poor fit-up conditions, even at elevated preheating currents.

Kang et al. [25] conducted experimental validation of theoretical analyses on constant current control (CCC) and constant power control (CPC) in welding processes. The results indicated that CCC outperforms CPC, as the latter is subject to a higher number of interfering variables. Furthermore, dynamic resistance analysis demonstrated that CCC supports a more reliable welding process, enabling earlier detection of the initial melting point compared to CPC. This experimental validation provides valuable insights for practical welding production, guiding welders in selecting an appropriate control strategy and contributing to enhanced energy efficiency in welding applications.

Xia et al. [26] introduced a novel approach to nondestructive measurement of weld penetration in robotic RSW. Their study involved in-depth analysis of electrode displacement signals through mechanism analysis and feature extraction. The reliability of these signal features was evaluated under normal and abnormal manufacturing conditions. Furthermore, they established an analytical model to predict weld penetration using physical modeling, which facilitates online measurement.

Zhou et al. [27] conducted a study focusing on the characteristics of the RSW process and the fundamental principle of electrical resistivity. They developed a comprehensive mathematical description for measuring the electrical resistivity of molten nuggets. Subsequently, a series of experiments were conducted, involving RSW operations to acquire dynamic resistance data, online temperature measurements to determine the electrical resistivity of solid metals, and metallurgical analyses to ascertain the size of molten nuggets. This work contributes to the establishment of accurate mathematical models for the RSW process, thereby aiding in welding automation, related research endeavors, and practical production processes.

In their study, Xia et al. [28] presented a novel approach for the online evaluation of expulsion intensity in RSW. By employing an advanced multi-sensor monitoring system and high-speed camera, they simultaneously monitored dynamic resistance, electrode force, and electrode displacement signals to analyze their instantaneous features. The experimental results revealed that the magnitude of the sudden decrease in force and displacement signals correlates with the expelled metal's weight, while no clear relationship was found between the sudden drop in resistance and expulsion severity. Further analysis established that sudden variations in electrode force serve as an optimal indicator for accurately assessing expulsion magnitude in servo gun systems.

Nazir et al. [29] proposed a comprehensive online tool condition monitoring (TCM) system for ultrasonic metal welding (UMW) that leverages sensor fusion and machine learning (ML) techniques. They engineered a data acquisition (DAQ) system to gather in-situ sensing signals throughout the welding process. From this data, a large pool of features was extracted, and a subset was selected for machine learning classification. Several classification models were trained, validated, and tested with experimental data, achieving near-perfect classification accuracy, nearly 100%, for both training and testing datasets.

In the study by Lee et al. [30], the focus is on developing a real-time online monitoring and diagnosis framework for angular misalignment in robot spot-welding systems. Data is collected using voltage and current sensors, capturing the associated mass data under both normal and abnormal (angular misalignment) conditions. Two categories of features are extracted: dynamic resistance (DR) features and voltage and current features decomposed by wavelet transform. Three types of critical feature sets—DR features, wavelet transform features, and hybrid features combining both—are prepared to train machine learning-based models. Support vector machine (SVM) and probabilistic neural network (PNN) are applied to establish the diagnosis models, and their diagnostic accuracy and robustness are evaluated.

El-Sari et al. [31] investigated the ability of multi-layer perceptron regression models to extrapolate, applying them with data markedly different from the training data in material and coating composition to predict nugget diameter based on process data. The study found that models which included features from the dynamic resistance curve performed better than those based solely on process parameters. This highlights the beneficial influence of process signals on the predictive precision and stability of ANN algorithms, particularly for datasets beyond the original training range.

Chino et al. [32] developed a nugget model for RSWs and extended the inherent strain method to predict RSW deformation quickly. Deformation induced by RSW involves electrical-thermal-mechanical coupling analysis, which is complex and time-consuming. Furthermore, using the inherent strain method, they efficiently predicted the deformation of a vehicle part with 23 RSWs in approximately 90 minutes, demonstrating good accuracy compared to measurements.

Hua et al. [33] have developed an in-situ ultrasonic detection system for automatic evaluation of RSW quality. This system utilizes an embedded probe to capture UT signals from spot welds post-RSW. Various signal eigenvalues, including acoustic pressure amplitude, echo distance, main frequency, main frequency amplitude, and low-frequency component, are obtained. Corresponding mathematical calculation models are established to enable quantitative ultrasonic evaluation of RSW quality. Additionally, specialized evaluation software has been developed to automatically calculate nugget sizes and classify weld types.

## 3. Methodology

The RSW process in the BIW stage of this automobile manufacturing involves welding sheet metal components by applying voltage and electric current through a copper alloy electrode, generating heat to create a weld nugget. This critical process in monocoque assembly is carried out automatically using robotic arms for precision and consistency. The main equipment is robotic welding guns. Weld quality is ensured through both destructive and non-destructive testing, including UT and a destructive method called teardown. These methods help increase efficiency, safety, and cost-effectiveness, allowing for high-speed production and strong, reliable welds essential for vehicle safety and

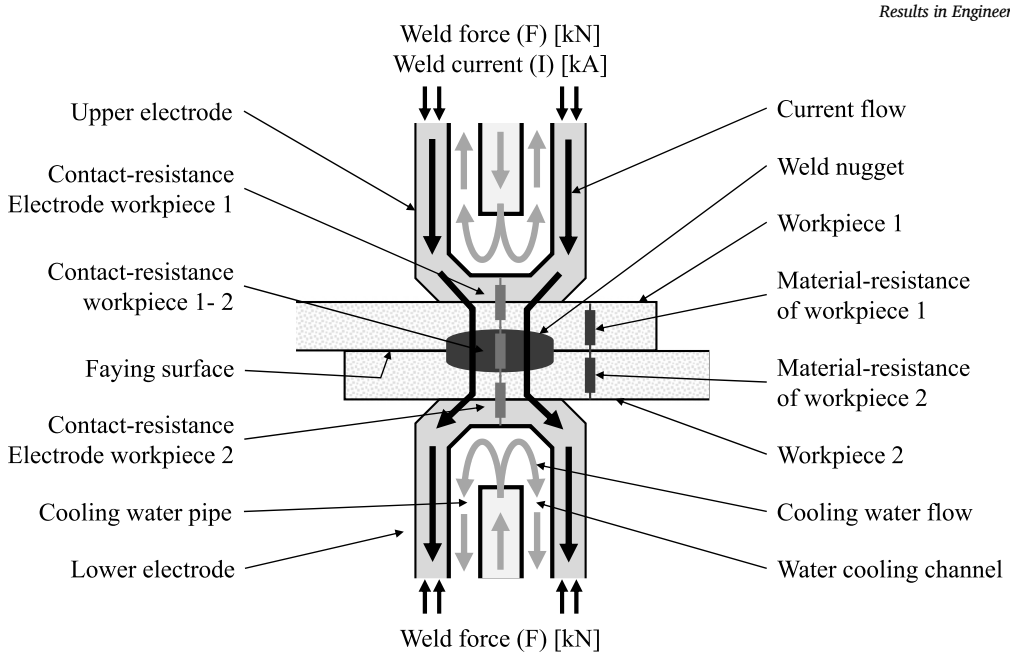


**Fig. 1.** A schematic of the metal RSW process [34].

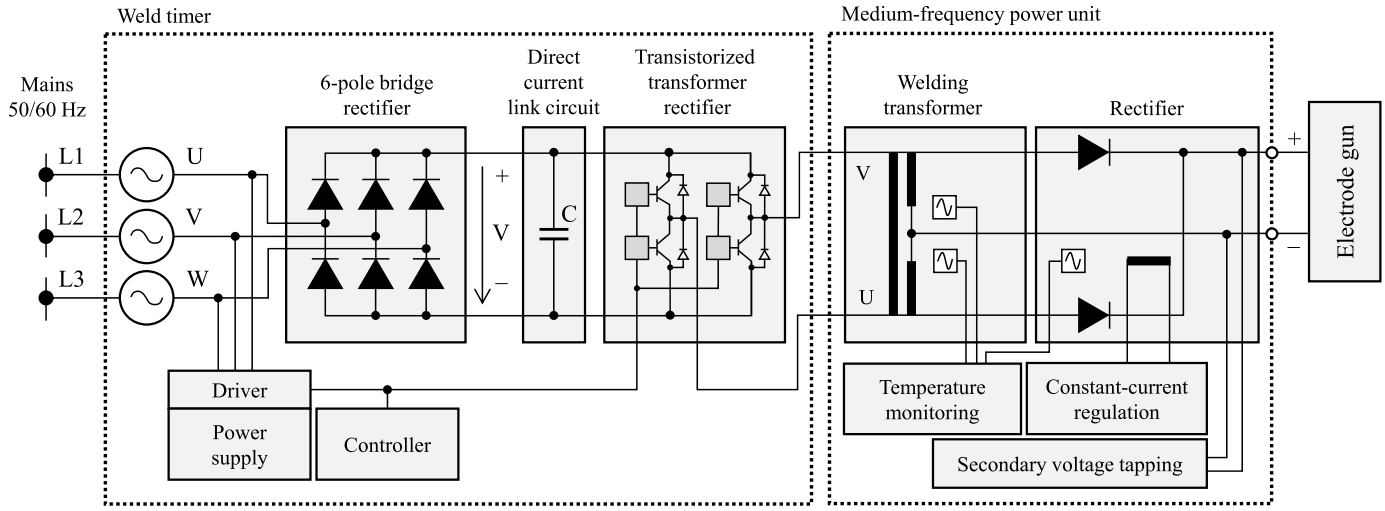


**Fig. 2.** WT and MF inverter diagram [10].

structural integrity. This article focuses solely on the robotic RSW process and non-destructive testing using UT, enabling data extraction from welding machines and measuring devices for modeling. In contrast, the teardown method provides only pass/fail results without additional information, which is why the selected devices are used for data retrieval.

### 3.1. Resistance spot welding

RSW is a cost-effective method for joining metals, relying on heat energy and pressure to create welds. The basics involve applying heat energy and pressure to reach the plastic state of materials, with factors such as pressure, current, and weld time playing essential roles. Metal transitions from a solid state to a partially liquid state and halted before full liquefaction to prevent expulsion and ensure weld integrity. Careful control of these parameters allowed RSW to produce strong, reliable welds for various applications. The term RSW originates from the electrical resistance of metals generating heat when current flows through them, leading to the formation of welding nuggets as the workpieces melt and solidify upon cooling. Different metals require varying degrees of control due to their unique characteristics, highlighting the importance of understanding and managing the process parameters for successful resistance welding, as shown in Fig. 1.

The RSW experiments were conducted using a robotic RSW consisting of an RK robot model, and an RO C-type servomotor driven with a B6 unit, as shown in Fig. 2. The B6 includes a weld timer (WT) and a medium-frequency power unit (MF inverter). The tasks of the MF inverter include generating the required current and weld time, as well as controlling the MF inverter itself. Meanwhile, the tasks of the WT involve controlling, regulating, and monitoring all programmed welding schedules, including message (status and errors), logging (recording every millisecond), and operation. Additionally, the WT facilitates communication with devices on the same process level via I/O connection, such as the robot, PLC (Programmable logic controller), control panel, and records the results in the form of an RUI file (a Bosch-designated file extension where 'R' stands for resistance, 'U' for voltage, and 'I' for current). These various equipment components work together to control the current delivered to the final device, the welding gun.

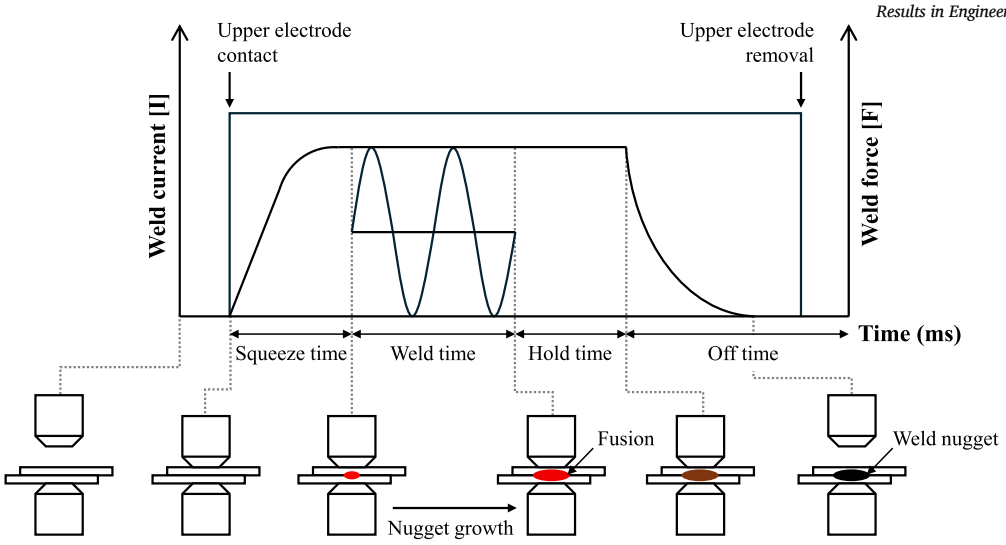


**Fig. 3.** Process parameters for RSW [35].

The welding standards follow ISO 14373:2015 which outlines the requirements for RSW in the assembly of uncoated and coated low carbon steel. Two identical dome-shaped F-type chromium-zirconium copper electrodes (ISO 5821, 2009) with a tip diameter of 6 mm were used, positioned as the upper and lower electrodes. Fig. 3 explains a typical basic RSW sequence. Critical to the proper formation of the weld nugget between the metal workpieces being welded are factors such as the resistance of the metal, the weld current, the duration of the current flow, and the welding force that compresses the workpieces together. The duration for which the welding current flows through the two workpieces of metal to be welded is particularly crucial. The following definitions may aid in understanding this drawing:

Squeeze time is the initial parameter between weld force and weld current. It must match mechanical motion. The instrument in this research allows adjustable parameters of 100–300 ms.

Weld time is the duration of weld current applied to the workpiece. Understanding the material helps in selecting the right time. The adjustable parameter range is 200–700 ms.

Hold time is the duration after weld current stops, maintaining weld force to solidify the weld nugget before releasing the parts. This parameter can be adjusted from 100–400 ms.

Off time is the period when the electrodes are not in contact with the workpiece during a repetitive welding cycle. It's necessary for moving the work between weld sequences. The necessary time to start the next weld process for the basic welding cycle, including the pre-heating time (Y), upslope time, and downslope time, is determined.

### 3.2. Ultrasonic testing

The RSW inspection tool used is the Tessonic brand, model F1, featuring 52 coaxial channels for estimating nugget diameter and indentations from the specimen. It is powered by an Intel® Atom N270 1.6 GHz processor and employs high-frequency sound waves to detect flaws, measure material thickness, and evaluate the internal structure of the test object. This tool supports both automatic and manual nugget size estimation and detection, with a scanning depth suitable for metal plates with thicknesses ranging from 0.6 to 2.4 mm. It is compatible with various materials, including mild steel, high-strength steel, dual-phase ultra-high-strength steel, and aluminum. The F1 can detect materials with and without coatings, such as zinc coatings (galvanized, galvanneal), e-coating, and paint. It is a portable and user-friendly device capable of producing images of spot welds' internal structures. In addition to welding images, this device detects cracks and inclusions, lack of fusion, and estimates the nugget diameter, shape, orientation, and thickness of the weld and the heat-affected zone (HAZ). It compares these measurements with predefined minimum nugget requirements to ensure that welds comply with industry standards, codes, and regulations, such as those from ASME, AWS, and ISO.

The F1 collects data from the surface and internal structures of the nugget. Special algorithms use this data to reconstruct the image of the spot weld and estimate the average diameter of the nugget area in real time. For this reason, this car manufacturing company uses the UT F1 equipment to evaluate welding quality. The equipment displays images and graphs from wave transmission to measure the size and thickness of the weld to judge its quality.

### 3.3. Methodology

For this research to yield high-quality components and achieve optimal results in model design, the dataset used to build the model is paramount. Accurate research results and maximum modeling values depend on proper data collection and preparation procedures. Furthermore, selecting the appropriate algorithm, model tuning, and employing data analysis tools, as well as methods for developing the model to be most efficient, are critical. Fig. 4 illustrates a flow chart with all the details of this research process.

1) Data source

Data is collected from two sources: experimental settings and actual production line data. The experimental data, obtained from spot welding on defined workpieces, resulted in a dataset of 450 points under the setting parameters of current and weld time. Meanwhile, the actual production line data was collected, totaling 120 points. The experimental datasets will be used to create the model, while the real data from the production line will be utilized to enhance the model for actual deployment in the production line. The next step involves the RSW process, where data from both sources will undergo the same procedures.

2) RSW process

This process starts with the robot receiving a command from the PLC to weld at the specified position. After completing the welding process, we have written a program in Python, using Jupyter Notebook, to read the RUI file and check the completeness of the weld data to determine if the process is complete, as standard programs cannot read this file type.

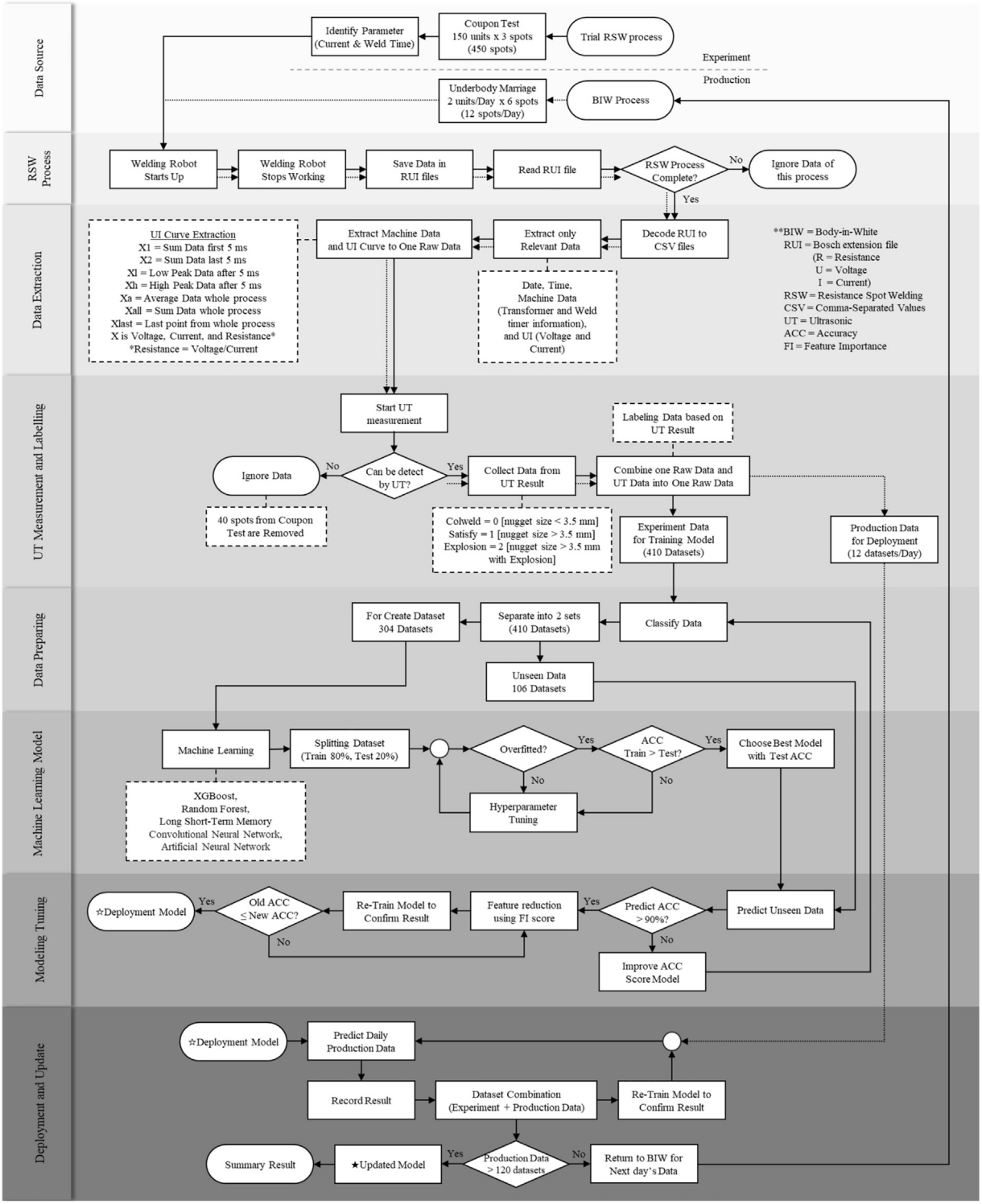


**Fig. 4.** Algorithmic procedure overview.

3) Data extraction

After extracting the necessary information, such as the date and time the process starts, voltage, current, voltage factor, current factor, and time spent in the welding process, these values are calculated. Subsequently, the voltage, current, and resistance values are plotted against the time spent in the welding process. The resulting graphs are used as one of the parameters in the dataset to build the model.

4) UT measurement and labeling

0.5 percent of the welding work will involve using a UT machine to measure the size of the welding spots in the front/rear floors. According to the company's standards, there are specific nugget size specifications for the front/rear floors, which will be used to classify welding quality into three levels. From this step, the production line data set detected welds that met all three levels at all 120 points. However, while the

experimental data set totaled 450 points, only 410 welds were found to meet the criteria.

5) Data preparing

In this step, we take a total of 410 datasets, and randomly divide them into two sets. The first set consists of 70% (274 datasets) used for building machine learning models, while the second set, comprising 30% (136 datasets), is used to validate the model as unseen data.

6) Machine learning model

The model dataset (274 datasets) was randomly divided into two parts, with 80% of the dataset used for training the model and 20% used for testing the model's accuracy. The best model was then selected from five different algorithms: ANN, CNN, LSTM, RFC, and XGBoost, considering conditions to prevent model overfitting.

7) Modeling tuning

The best model is used to make predictions with unseen data (136 datasets), ensuring that the model's accuracy is no less than 90%. If the accuracy falls below this threshold, the process will revert to the data preparation step to randomly redistribute all the 410 datasets. This is necessary due to the limited dataset available for model building. The same dataset must be reused, allowing for random reallocation to find the best model from the optimal dataset division. Feature engineering (FE) techniques are employed to enhance model efficiency by reducing less important features or parameters using feature importance (FI) score, ensuring that the model's accuracy is not less than the most recent value obtained. This process continues until the best final model is achieved, ready to be deployed in real situations, such as the production line.

8) Deployment and update

From this step, the model is developed daily based on real data. First, we will test the model using 12 datasets from the production line in one day. All 12 datasets undergo the same data preparation process as the experimental datasets mentioned above. These datasets are used to make predictions and record the results for follow-up data collection. The 12 datasets are then combined with the previous 274 train datasets, creating a total of 286 datasets, which are re-trained to allow the model to learn. This process continues for 10 days, resulting in 120 datasets from the production line, a total of 394 datasets. The final data is recorded, and the results are summarized.

### 3.3.1. Database analysis

The BIW process involves assembling the main parts to form a monocoque, including the dash compartment, floor panel carrier system, rear compartment, roof, and left-right side frames using the RSW method. In this article, we have collected information from a model TA pickup truck. The connection points of interest are between the front compartment (dash compartment welded assembly with floor panel carrier system) and the rear compartment. Both compartments, when welded together, are referred to as the "front/rear floor". These points are critical for safety as they support the entire weight of the cabin and the vehicle's drivetrain. After completing the welding process, the next step is to randomly select cars from the total produced each day. On average, the factory produces over 400 monocoques per day in the BIW process. Two car bodies are randomly selected each day for UT inspection to measure the weld nugget size. The remaining car bodies are sent directly to the painting process. If the UT inspection reveals that the nugget size does not meet the factory standards, the chassis is sent to a specialized repair department for adjustments before returning to normal production for the painting process. Fig. 5 shows the steps within the BIW process.

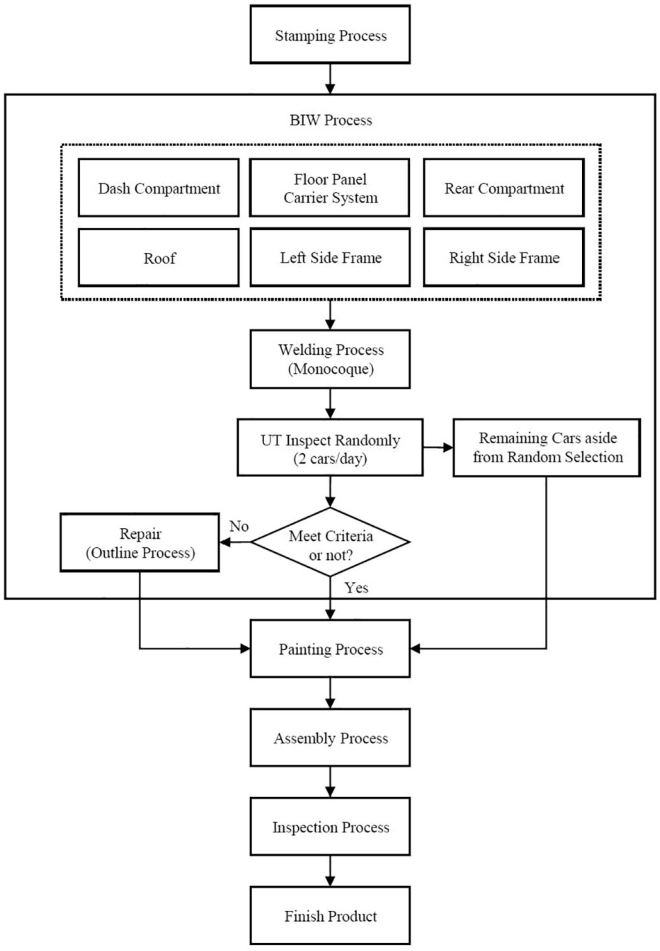


**Fig. 5.** Step in the BIW process.

### 3.3.2. Dataset

The obtained data must undergo several steps before it can be utilized. Starting from extracting raw data from WT, we select relevant data, such as removing constant values and irrelevant text that cannot be converted to usable numbers. The data is then organized into sets or groups with similar properties according to the specified structure or class, which will be used to train the algorithm to create a model. A high-quality dataset is valuable to both the data provider and the user. Therefore, we will focus on the method of obtaining the initial data first. As mentioned above, there are two groups of data sources: from experiments and production processes involving RSW between two workpieces of HSS-type (high tensile steel) metal. Each steel plate is 0.7 mm thick (with a tolerance of -0.02 mm) and coated with galvanization. This steel type withstands a tensile force of 270 MPa. The details and sources are discussed in the next section below.

*3.3.2.1. Experiment dataset* In the present era, technology has developed significantly to make work more efficient and reduce errors. The robotic RSW methods are a prime example of this advancement. It has been modernized to minimize mistakes and is extensively used in critical areas concerning structure and user safety. Processes are designed with precision and high standards. However, no system is perfect; over time, the deterioration of machinery or the properties of the material itself can affect welding quality. When mistakes occur, they can cause significant damage, especially in crucial parts or positions. Therefore, identifying problems before they escalate to the next process and promptly solv-

**Table 1**
Classification levels definition.

| Class level | Weld quality | Level condition | Dataset | |
|---|---|---|---|---|
| | | | Training | Unseen |
| Class 0 | Satisfy | Nugget size > 3.5 mm | 163 | 81 |
| Class 1 | Expulsion | Nugget size > 3.5 mm & Expulsion | 44 | 22 |
| Class 2 | Cold weld | Nugget size < 3.5 mm | 67 | 33 |

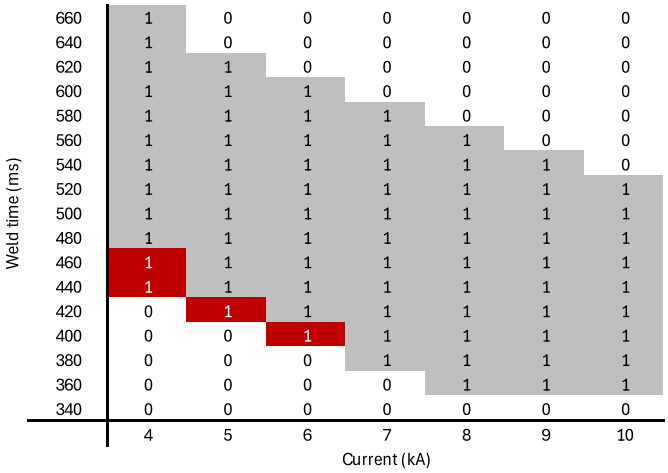


**Fig. 6.** RSW parameters setting using lobe curve technique.

ing them is essential and should be a primary focus. RSW mistakes are rare, resulting in almost no data. Therefore, it is necessary to conduct an experiment. The parameters affecting welding quality are the welding current and time. We designed the experiment to adjust both parameters, which can be set at WT before welding. We used the Lobe curve principle techniques [36] to define the range of settings, consisting of 75 parameter pairs as shown in Fig. 6, to be used for further model training. In the Lobe curve, a value of 1 indicates the parameter is used, while 0 means it is not. The red color of 1 indicates that, although the parameter pair is used, no weld nugget is formed between the workpieces due to insufficient current and weld time. The experimental setup included 150 specimens, each measuring 75x150x0.7 mm, cut from raw materials used in building real vehicles. Three spot welds were performed on each specimen, spaced 20 mm apart, resulting in raw data collection of 450 spot welds (150 specimens x 3 spot welds). However, 40 failed welds went undetected by UT, leaving 410 datasets for machine learning.

*3.3.2.2. Production dataset* The number of welding points on the front/rear floor totals nearly 90, with an equal number on each side. In this article, we will focus on the left-hand side, as both sides have identical welding requirements and are welded in the same positions, i.e., symmetrically. Of the total welding points on both sides, 17 are on 2 workpieces, and 27 are on 3 workpieces. For the scope of this research, we will only consider the welding points on 2 workpieces. A total of 8 RSW welding robots (4 per side) are used to weld all the points, with each robot responsible for different positions and numbers of welding points. This research specifically studies and extracts data from the fourth welding robot, an RK model, which performs 17 welding points (including 13 on 2 workpieces and 4 on 3 workpieces) on the left-hand side. In designing the welding points, allowances have been made for critical and additional welding points. Therefore, we will focus on the 6 critical welding points on 2 workpieces out of the 13 handled by the fourth welding robot. Data from the BIW process for the front/rear floor parts were collected daily over ten days (2 cars/day), totaling 120 spot welds (20 cars x 6 weld spots per car), all of which met the criteria according to the UT method.

### 3.3.3. Fault types

Weld quality guarantees the integrity and overall characteristics of the welding assembly during production. Maintaining high-quality welds is crucial to ensure the reliability and safety of the welded structure or component. There are eight types of weld quality: satisfactory (meets engineering requirements), undersized (dimension less than satisfactory), discrepant (below undersized), edge (weld located beyond trim edge), missing (weld not present as specified), off location (weld not within a 10 mm radius of the specified location), expulsion (splatter at the spot point).

For our study, we will focus on four weld quality categories: satisfactory, undersized, discrepant, and expulsion. These will be classified into three levels using machine learning. The details for each level are as follows:

**Level 0: Satisfy**

This level describes welding quality that meets the engineering principles and requirements of this factory, specifically requiring a nugget size greater than 3.5 mm.

**Level 1: Expulsion**

This level includes the expansion of molten material between the electrode tip faces, where excessive expulsion is undesirable. The nugget size remains within standard, specifically greater than 3.5 mm, with scattered welding flakes present.

**Level 2: Cold weld**

This last level combines two types of weld quality: undersized and discrepant, both of which indicate a weld size requirement of less than 3.5 mm nugget size.

After establishing the criteria, we will apply these standards to classify datasets obtained from both experimental setups and the production line into categories based on welding quality levels, as illustrated in Table 1. Fig. 7 displays the C-scan areas obtained from the UT for all three welding quality classes. These C-scan images are generated from the collected measurement data, highlighting different regions of fusion within the weld. The green areas indicate regions where proper fusion has occurred, while the red areas represent regions with no fusion. This visual representation helps in distinguishing between satisfactory welds, expulsion, and cold welds.

### 3.3.4. Feature extraction

In the data exported from an RSW robot, we can extract data from the WT in RUI format and convert it to a CSV file using Python. After conversion, we selected the required data, including the datetime of the process start, voltage (V), current (I), energy during RSW (BEnergy), heat during RSW (BPmax) and time spent in the welding process (Weldtime). Additionally, values include the current factor (Ifactor) and voltage factor (Vfactor) obtained from the MF inverter, along with calculated parameters like heat value. Using a voltage and current values, we can calculate resistance according to Ohm's Law, which states that I is directly proportional to V and inversely proportional to resistance (R). The relationship between V, I, and R is expressed in Equation (1).

$$R = \frac{V}{I} \tag{1}$$

During RSW welding, Joule's first law illustrates the relationship between the heat produced and the flowing electric current through a conductor. Here, Q represents the amount of heat, and T represents time, as shown in Equation (2).

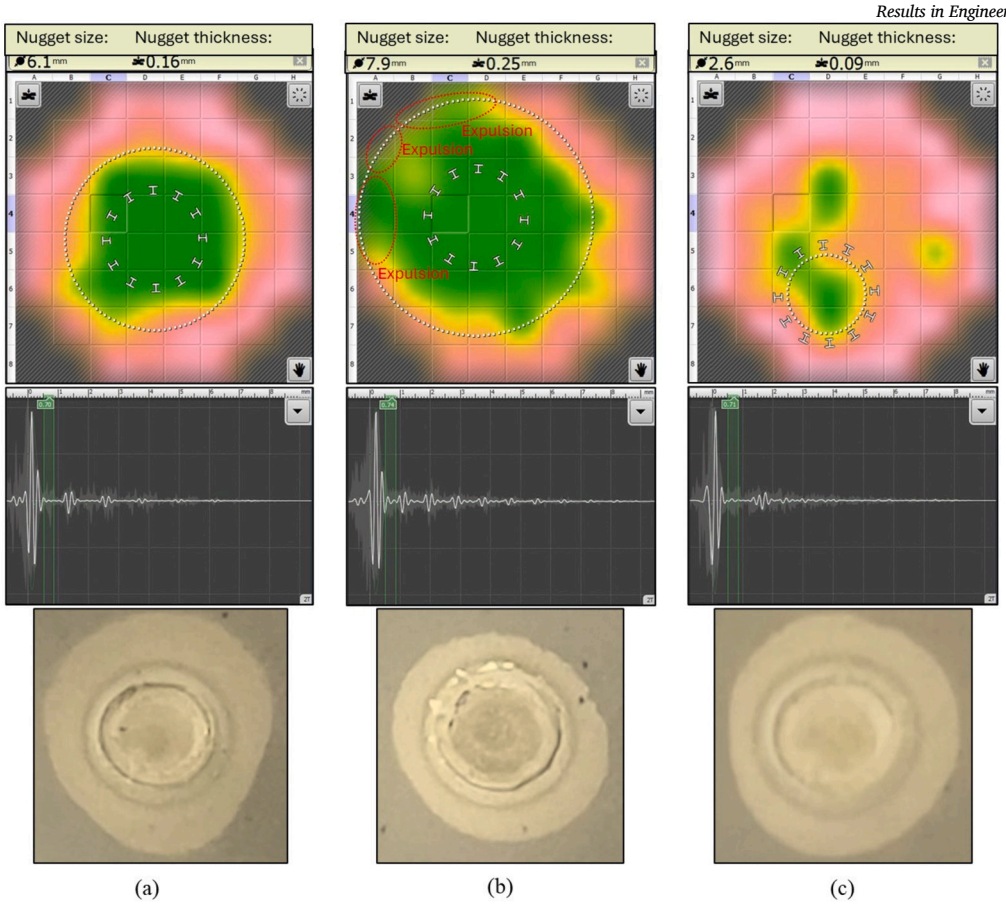


**Fig. 7.** C-scan area for each weld quality. (a) Satisfy, (b) Expulsion, (c) Cold weld.

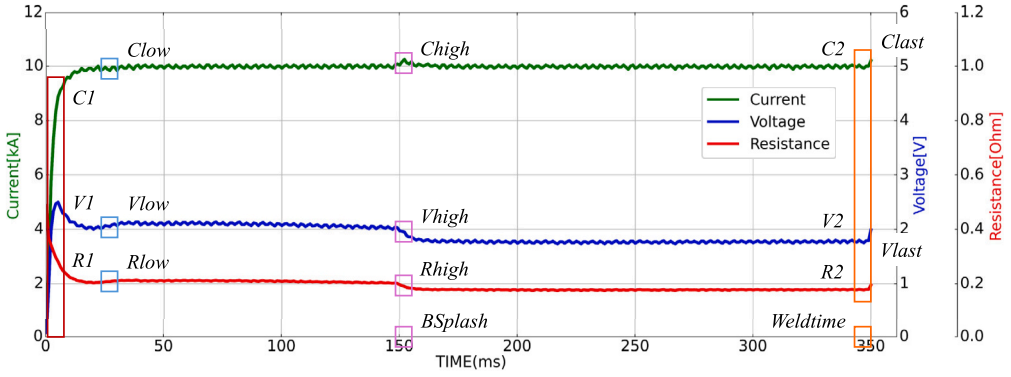


**Fig. 8.** Graph of voltage, current, and resistance during welding.

**Table 2**
Parameter differences analysis (95% CI).

| No. | Parameter | P-value | Significant |
|---|---|---|---|
| I | BWear | 0.273932 | No |
| II | Weldtime | 0.004022 | Yes |
| III | R1 | 0.223971 | No |
| IV | Clast | 0 | No |
| V | Vall | 0.017031 | Yes |
| VI | Ra | 0 | Yes |

$$Q = I^2 RT \tag{2}$$

The total energy (E) consumed during resistance spot welding is calculated by integrating the product of V and I over the welding time (t), as expressed in Equation (3). This calculation differs from BEnergy, which excludes the high value at the last point on the graph (Fig. 8). The WT records data from the secondary circuit using embedded voltage and current sensors, capturing values every millisecond for heat and energy calculations in the weld timer. According to Joule's first law, heat and energy are essential for nugget formation: insufficient heat results in weak joints, while excessive heat can cause defects such as over-fusion. These parameters are critical inputs for the machine learning model, which uses them to predict weld quality based on calculated heat input, enhancing predictive accuracy in determining the likelihood of producing a quality weld.

$$E = \int_0^T V(t) \times I(t)\, dt \tag{3}$$

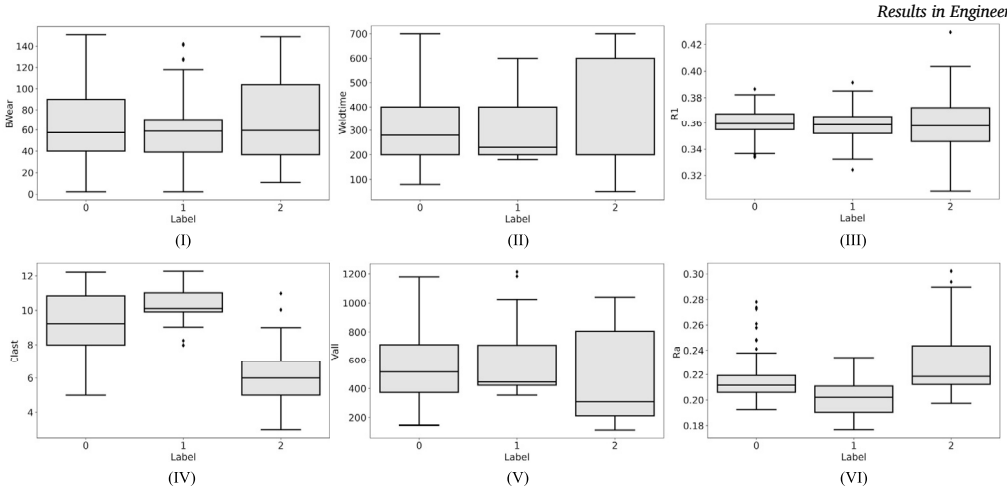


**Fig. 9.** Box plot analysis of 6 sample parameters across weld quality levels.

The voltage, current, and resistance values were plotted against the time spent in the welding process. From the obtained graph, shown in Fig. 8, various statistics were calculated to serve as parameters in the dataset used to build the model. These parameters include the mean of the first 5 milliseconds, the mean of the last 5 milliseconds, the maximum value after the first 5 milliseconds, the minimum value after the first 5 seconds, the overall average, the total sum, and the final value of the graph. One dataset obtained from the WT corresponds to one connection point on the front/rear floor. There are 31 parameters in total, but which parameters can be used to build the model? Although every parameter is related to the RSW process, it is necessary to test and analyze the relationship between the independent variable and the dependent variable. The method we use is one-way ANOVA. Here, variables are groups of datasets classified into levels, and the dependent variables are all 31 parameters that were collected. In the process of testing, we will formulate hypotheses as follows:

*Null hypothesis ($H_0$):* The average values of the datasets at each level of welding quality are not different.

*Alternative hypothesis ($H_1$):* The average values of the datasets for each level of welding quality are different.

We have set a significant level of 0.05 or 95% confidence interval. The results of analyzing the mean of each dataset at all three levels of weld quality with a P-value greater than 0.05 means that ($H_0$) is accepted, indicating that the variances of each dataset across at least two groups are the same and therefore will not be considered. Fig. 9 shows the results of the analysis of the dataset for each weld quality level in a box plot format, compared with the results of the one-way ANOVA analysis as shown in Table 2, using 6 parameters as examples. From a total of 31 parameters, the summary results from the analysis found that three parameters, namely BWear, and R1, will be eliminated, leaving a total of 29 parameters to continue building the model as shown in Table 3.

### 3.3.5. Artificial neural networks

ANN were selected for their ability to learn intricate patterns in data, particularly when predicting outcomes from nonlinear relationships, which are common in complex manufacturing processes like RSW. The dataset used for training ANNs consisted of both structured (e.g., welding parameters, environmental conditions) and unstructured data (e.g., images, sensor readings), with features capturing both static properties (material type) and dynamic attributes (current, pressure, time). Preprocessing included scaling and normalization to ensure that features fed into the network were on a comparable scale, enhancing the model's convergence during training.

**Table 3**
Model training dataset parameters.

| Parameter | Unit | Meaning description |
|---|---|---|
| R | mΩ | Resistance (from equation (1)) |
| Q | J | RSW heat (from equation (2)) |
| E | J/s | Energy (from equation (3)) |
| Ifactor | - | Curent factor of MF inverter |
| Vfactor | - | Voltage factor of MF inverter |
| BEnergy | J/s | Energy using during RSW |
| BPmax | J | Heat using during RSW |
| BSplash | ms | Time at high peak current |
| Spatter | - | Status *(0, 1) of BSplash |
| Weldtime | ms | Weld time (refer to Fig. 3) |
| C1 | kA | Average current first 5 ms |
| C2 | kA | Average current last 5 ms |
| Ca | kA | Average current |
| Call | kA | Sum current |
| V1 | V | Average voltage first 5 ms |
| V2 | V | Average voltage last 5 ms |
| Va | V | Average voltage |
| Vall | V | Sum voltage |
| R2 | mΩ | Average resistance last 5 ms |
| Ra | mΩ | Average resistance |
| Rall | mΩ | Sum resistance |
| Chigh | kA | High peak current after 5 ms |
| Clow | kA | Low peak current after 5 ms |
| Vhigh | V | Voltage at Chigh |
| Vlow | V | Voltage at Clow |
| Rhigh | mΩ | Resistance at Chigh |
| Rlow | mΩ | Resistance at Clow |
| Clast | kA | Last value of current |
| Vlast | V | Last value of voltage |

*0: No high peak current (no BSplash).
1: High peak current (has BSplash).

Hyperparameter tuning involved adjusting the number of hidden layers, the number of neurons per layer, learning rates, and activation functions (such as ReLU in hidden layers and softmax in the output layer). Regularization techniques like dropout and L2 regularization were applied to prevent overfitting. The backpropagation algorithm, along with the Adam optimizer, was used to adjust weights, minimizing the loss function iteratively and improving predictive accuracy. This setup allowed the ANN to generalize well across diverse weld quality scenarios, enhancing its robustness in prediction.

### 3.3.6. Convolutional neural networks

CNN were incorporated to handle image-based and spatial data, essential in analyzing surface defects or weld geometry that are indicative of weld quality. The CNNs were configured to learn spatial hierarchies within images using convolutional layers, which extracted feature maps

representing weld quality attributes (e.g., seam uniformity, porosity indicators). Preprocessing involved resizing, normalization, and data augmentation (rotation, flipping, and scaling) to increase the variability and robustness of the model in handling weld image inconsistencies.

Hyperparameter tuning for CNNs included adjusting filter sizes, the number of filters per layer, learning rate, and the dropout rate to optimize performance. Cross-validation and a grid search approach were used to identify the best combinations of these parameters. Pooling layers were incorporated after each convolutional layer to reduce the feature dimensions, preventing overfitting and speeding up computation. By leveraging parameter sharing and local connectivity in convolutional layers, the CNNs were able to process high-dimensional image data effectively, contributing to accurate weld quality classification.

#### 3.3.7. Long short-term memory

LSTM were selected to model temporal dependencies and trends in sequential data, such as time-series sensor data, current, or pressure sequences that evolve during the welding process. This model was essential for capturing how past welding cycles or temporal changes affect current quality predictions. The dataset for LSTM consisted of sequences reflecting the chronological order of welding steps, where each sequence element represented a timestamped value of the variables under consideration. Preprocessing involved sequence padding to standardize input lengths and normalization to improve model convergence.

To optimize LSTM performance, hyperparameter tuning was performed on parameters like the number of LSTM units, learning rate, and dropout rate. Gate mechanisms within LSTM cells (input, forget, and output gates) managed the information flow, allowing the model to retain or forget information as necessary, essential in preventing the vanishing gradient problem. An Adam optimizer was employed to adjust weights iteratively, and LSTM depth was varied to identify an optimal architecture capable of accurately capturing the temporal patterns critical for weld quality prediction.

#### 3.3.8. Random forest classifier

The Random Forest Classifier (RFC) was selected for its robustness in handling complex datasets with high dimensionality and noise, which are common in welding process data. This ensemble model effectively handled various feature types (categorical, numerical) present in the dataset, from material specifications to environmental factors impacting weld quality. Preprocessing involved handling missing values and converting categorical variables using one-hot encoding, ensuring each tree received a consistent, high-quality data input.

Hyperparameter tuning focused on the number of trees in the forest, maximum tree depth, minimum samples per leaf, and the number of features considered per split. A grid search method helped in identifying the optimal parameter combinations, enhancing the model's performance while minimizing overfitting. The RFC aggregated predictions from multiple decision trees, providing robust and reliable classifications, particularly valuable for understanding complex feature interactions in weld quality assessment.

#### 3.3.9. Extreme gradient boosting classifier

Extreme Gradient Boosting (XGBoost) was selected for its efficiency and high predictive accuracy, making it suitable for capturing complex interactions among welding parameters and environmental factors. The model leveraged advanced gradient boosting techniques to iteratively minimize prediction errors. The dataset characteristics included various types of features, all of which were preprocessed through normalization, encoding, and feature engineering to enhance signal clarity and model effectiveness. Feature selection played a crucial role, reducing the dimensionality to only the most predictive, improving both the model's accuracy and interpretability.

Hyperparameter tuning for XGBoost included optimizing the learning rate, maximum tree depth, subsampling ratio, and the L1 and L2 regularization parameters to control overfitting. Grid and random search methods were employed to fine-tune these hyperparameters. The model's efficiency was further enhanced by tree pruning (to prevent overcomplexity) and parallel processing (to speed up training). With XGBoost's adaptability and precision, the model achieved high predictive performance, accurately identifying patterns indicative of weld quality and significantly outperforming other models in terms of precision and recall.

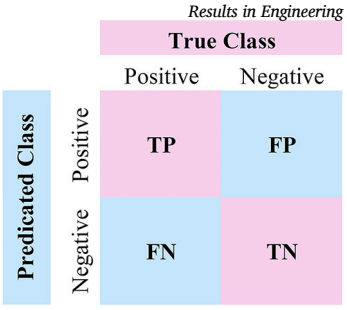


**Fig. 10.** Typical structure of confusion matrix.

### 3.4. Performance metrics

Using default algorithms for modeling is generally acceptable, but it is crucial to carefully evaluate whether their results are correct and suitable. Each algorithm is designed to fit different types of datasets, such as classification, regression, or clustering, each with unique characteristics depending on how the data was sourced. Considerations like data collection methods and feature selection play vital roles. Selecting the right algorithm tailored to the dataset is the primary consideration. However, performance alone isn't the sole criterion. Overfitting can occur when model results seem excessively accurate training, potentially due to the dataset's limited diversity, causing the algorithm to learn noise or specific dataset details rather than general patterns. To mitigate this, additional datasets are often introduced to enhance machine learning—a common practice. Another effective approach is hyperparameter tuning, which involves adjusting values that control model complexity to strike balance against overfitting. Optimized parameters can significantly improve a model's ability to generalize to new, unseen data, thereby enhancing overall performance on a given dataset. Finding the right parameter combination that maximizes performance measures is critical for ensuring the model's reliability and practical utility. In our study, the initial results were promising. However, due to material constraints in our experiments, acquiring additional datasets for training wasn't feasible. Hence, we focused on adjusting parameters to optimize model performance. Table 4 presents the adjusted parameters for each model compared to their default settings. What is the best and most suitable machine learning model? This section discusses standard performance indicators used to evaluate a model's accuracy based on how well it predicts outcomes. These indicators are used to compare algorithms to select the best model, ensuring it meets standards of accuracy and reliability. The indicators used to evaluate models categorized into discrete classes include accuracy, precision, recall, and F1 score. These metrics are calculated using the values in the confusion matrix, as shown in Fig. 10, and are used to evaluate the performance of all four indicators as follows: Precision: Calculates the ratio of true positive predictions to the total positive predictions made by the model, as shown in Equation (4).

$$Precision = \frac{TP}{TP + FP} \tag{4}$$

Recall (Sensitivity or True positive rate): Calculates the percentage of actual positive instances that were correctly identified as positive, as indicated in Equation (5).

$$Recall = \frac{TP}{TP + FN} \tag{5}$$

**Table 4**
Hyperparameter comparison for default and tuned algorithm models.

| Algorithm | Hyperparameter | Default | Tuned |
|---|---|---|---|
| ANN | output_size | 1 | 1 |
| | hidden_sizes | [128,64] | [1024, 512, 256, 128, 64, 32, 16, 8, 4] |
| | batch_size | 32 | 32 |
| | epochs | 10 | 2000 |
| | lr | 0.001 | 0.0005 |
| | dropout_rate | 0 | 0.2 |
| | Optimizer | - | Adam |
| | Criterion | - | CrossEntropyLoss |
| CNN | output_size | 1 | 1 |
| | batch_size | 32 | 32 |
| | epochs | 10 | 1000 |
| | lr | 0.001 | 0.0001 |
| | dropout_rate | 0.1 | 0.1 |
| | random_state | 10 | 10 |
| LSTM | output_size | 3 | 1 |
| | batch_size | 32 | 32 |
| | epochs | 10 | 100 |
| | random_state | 42 | 37 |
| | learning_rate | 0.001 | 0.0001 |
| RF | N_estimators | 100 | 12 |
| | Max_depth | 1 | 11 |
| | Min_samples_split | 2 | 2 |
| | Min_samples_leaf | 1 | 10 |
| | N_jobs | -1 | -1 |
| | Test_size | 0.2 | 0.2 |
| | Random_state1 | 0 | 7 |
| | Random_state2 | 1 | 48 |
| XGB | Max_depth | None | 8 |
| | N_estimators | 100 | 5 |
| | Random_state1 | None | 5 |
| | Random_state2 | 1 | 96 |
| | tree_method | None | GPU Hist |

F1 score: The harmonic mean of precision and recall, balancing both metrics, as demonstrated in Equation (6).

$$F1\ score = \frac{2 \times (Precision \times Recall)}{Precision + Recall} \tag{6}$$

Accuracy: Calculates the percentage of accurately predicted instances out of the total instances, as shown in Equation (7).

$$\text{Accuracy} = \frac{\text{TP} + \text{TN}}{\text{TP} + \text{TN} + \text{FP} + \text{FN}} \tag{7}$$

where:
True positive (TP) = A prediction that correctly matches the actual positive outcome.
True negative (TN) = A prediction that correctly matches the actual negative outcome.
False positive (FP) = A prediction that does not match the actual outcome, where the prediction is positive, but the actual result is negative.
False negative (FN) = A prediction that does not match the actual outcome, where the prediction is negative, but the actual result is positive.

The ROC (Receiver Operating Characteristic) curve will be used to visualize the trade-off between recall and false positive rates across different threshold settings. This helps in understanding how changing the decision threshold affects model performance. Different models can be compared, with the ROC curve closer to the upper left corner indicating better model performance. By comparing the ROC curves of multiple models, we can determine which model performs best under different criteria but with same dataset. Conversely, a model with a curve closer to the 45-degree diagonal (random chance line) shows poor performance. Additionally, we can calculate the AUC (Area Under the Curve), a single scalar value summarizing the model's overall performance. Higher AUC values indicate better model performance, making it a particularly useful metric for comparing models.

## 4. Experiments and results

Modelling to predict weld quality at three levels—Satisfy (Level 0), Expulsion (Level 1), and Cold weld (Level 2)—were created using five different algorithms. Three models were built using machine learning algorithms (LSTM, RF, and XGBoost), and the other two were built using deep learning algorithms (ANN and CNN) through hyperparameter tuning. These models were then compared. As shown in Fig. 11, the results from the five models are plotted using ROC curves along with their respective AUC values. The ROC curves for XGBoost, LSTM, RF, and CNN all closely approach the upper left corner, indicating strong model performance, with AUC values of 0.998, 0.990, 0.979, and 0.967, respectively. The ANN model, however, has a lower AUC of 0.859. The visual comparison of the ROC curves makes it easy to observe differences in model performance. When combined with the AUC values, it provides a clearer understanding of each model's effectiveness. However, determining the best model is challenging, as two models—LSTM and XGBoost—yielded almost equal results. Therefore, it is necessary to consider additional performance metrics, as shown in Table 5.

From the information in Table 5, it is evident that while models using default hyperparameters yield good results, there is still room for improvement through hyperparameter tuning. Using default hyperparameters does not entirely prevent overfitting. For instance, the default XGBoost model has a training accuracy (Train ACC) of 100%, but its testing accuracy (Test ACC) drops to 81.8%. Similarly, the default RF model has a Train ACC of 77.2% and a Test ACC of only 63.6%. Despite the high AUC-ROC scores of both models, which are over 0.9 and nearly on par with LSTM and CNN, they still manage to protect themselves from overfitting, much like the ANN model, which has the smallest AUC-ROC score. After proper hyperparameter tuning, XGBoost demonstrated the best overall performance, with a Train ACC of 99.5% and a Test ACC of 96.4%. The second-best model was the ANN, which, after tuning,

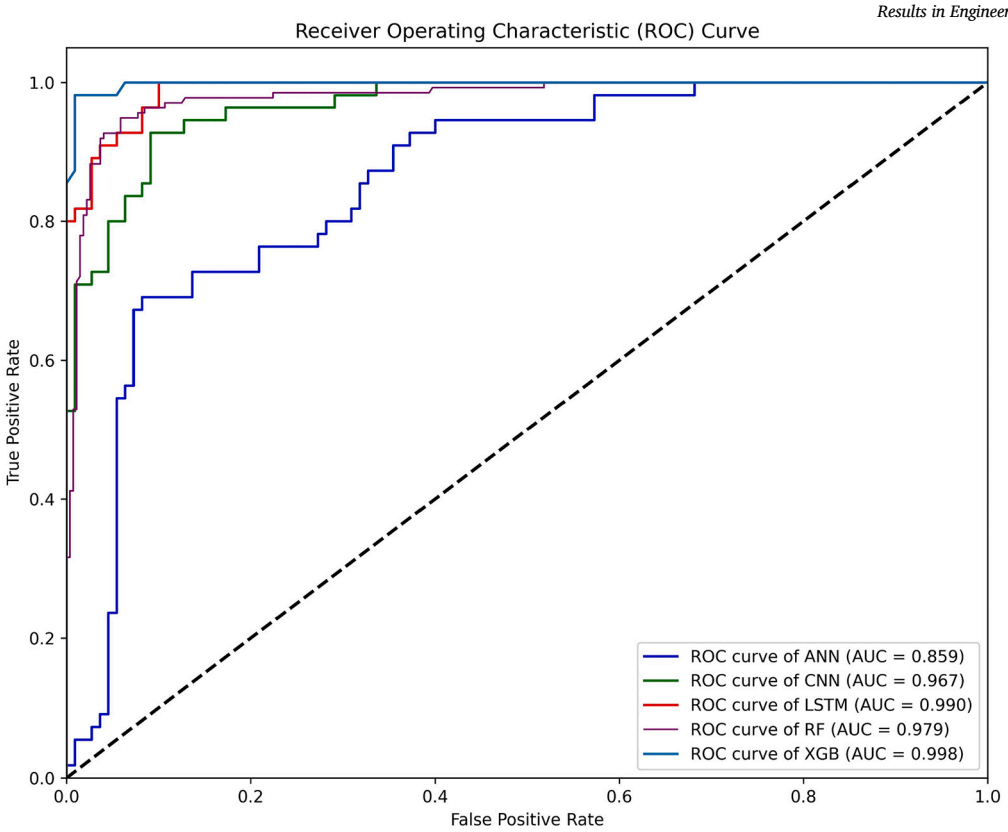


**Fig. 11.** ROC and AUC-ROC analysis comparison for five algorithm models.

**Table 5**
Performance metrics comparison between five algorithm models.

| Model | Type | Precision | Recall | F1-score | Train ACC | Test ACC | Unseen ACC |
|---|---|---|---|---|---|---|---|
| ANN | Default | 72.73 | 72.73 | 72.73 | 72.76 | 72.73 | 72.06 |
| | Tuned | 98.17 | 90.91 | 91.91 | 93.55 | 89.55 | 91.11 |
| CNN | Default | 69.09 | 69.09 | 69.09 | 72.60 | 69.90 | 69.85 |
| | Tuned | 94.52 | 92.73 | 93.38 | 92.73 | 92.73 | 92.73 |
| LSTM | Default | 81.30 | 76.36 | 76.99 | 84.02 | 80.88 | 76.36 |
| | Tuned | 92.50 | 92.73 | 92.37 | 98.17 | 92.73 | 92.65 |
| RF | Default | 55.88 | 63.64 | 57.68 | 77.17 | 63.64 | 75.00 |
| | Tuned | 92.24 | 90.91 | 91.91 | 88.76 | 90.21 | 89.42 |
| XGB | Default | 85.81 | 84.02 | 84.45 | 100.00 | 81.82 | 92.65 |
| | Tuned | 93.33 | 98.15 | 95.34 | 99.54 | 96.36 | 95.59 |

achieved a Train ACC of 98.6% and a Test ACC of 92.7%. This performance was closely followed by the LSTM model, which had Train ACC and Test ACC values of 98.2% and 92.7%, respectively. The RF model also showed significant improvement, with Train ACC and Test ACC values of 93.6% and 92.7%. The CNN model, while still effective, had the lowest performance among the tuned models, with a Train ACC of 97.3% and a Test ACC of 89.1%.

However, we are not completely satisfied with just considering the overall performance. We prioritize avoiding under-killed predictions over over-killed ones. This means we will not accept predictions that incorrectly classify a poor-quality weld as a good one, but we can tolerate predictions that correctly classify a good-quality weld as poor. Specifically, in our case, it is unacceptable if the model predicts a cold weld (Level 2) as satisfactory (Level 0). We will examine this further through the confusion matrix analysis of each model's predictions on unseen data, as shown in Fig. 12.

All models were able to predict the Expulsion (Level 1) class from unseen datasets with 100% accuracy. For the Satisfy (Level 0) class, all models similarly misclassified some datasets as Cold weld (Level 2), but none misclassified them as Expulsion (Level 1). As mentioned, we can tolerate over-killed predictions, especially when the error rate is below 7%, though ideally, it should be zero. Our primary focus is on avoiding under-killed predictions for Cold weld (Level 2). Among all the models, XGBoost made only one incorrect prediction out of 33 unseen datasets, achieving a prediction accuracy (Prediction ACC) of 95.6%.

In our evaluation of machine learning models for weld quality prediction, minimizing under-killed predictions—where poor-quality welds are classified as satisfactory—was our priority, while we tolerated over-killed predictions, where good-quality welds might be flagged as poor. This approach ensures the structural integrity of the final product by preventing faulty welds from being misclassified as acceptable. Below, we present a comparative analysis of the models tested, focusing on their ability to predict Cold welds (Level 2), which are critical for quality assurance.

ANN performed reasonably well across most classes but faced challenges in maintaining high specificity for Cold weld predictions. While

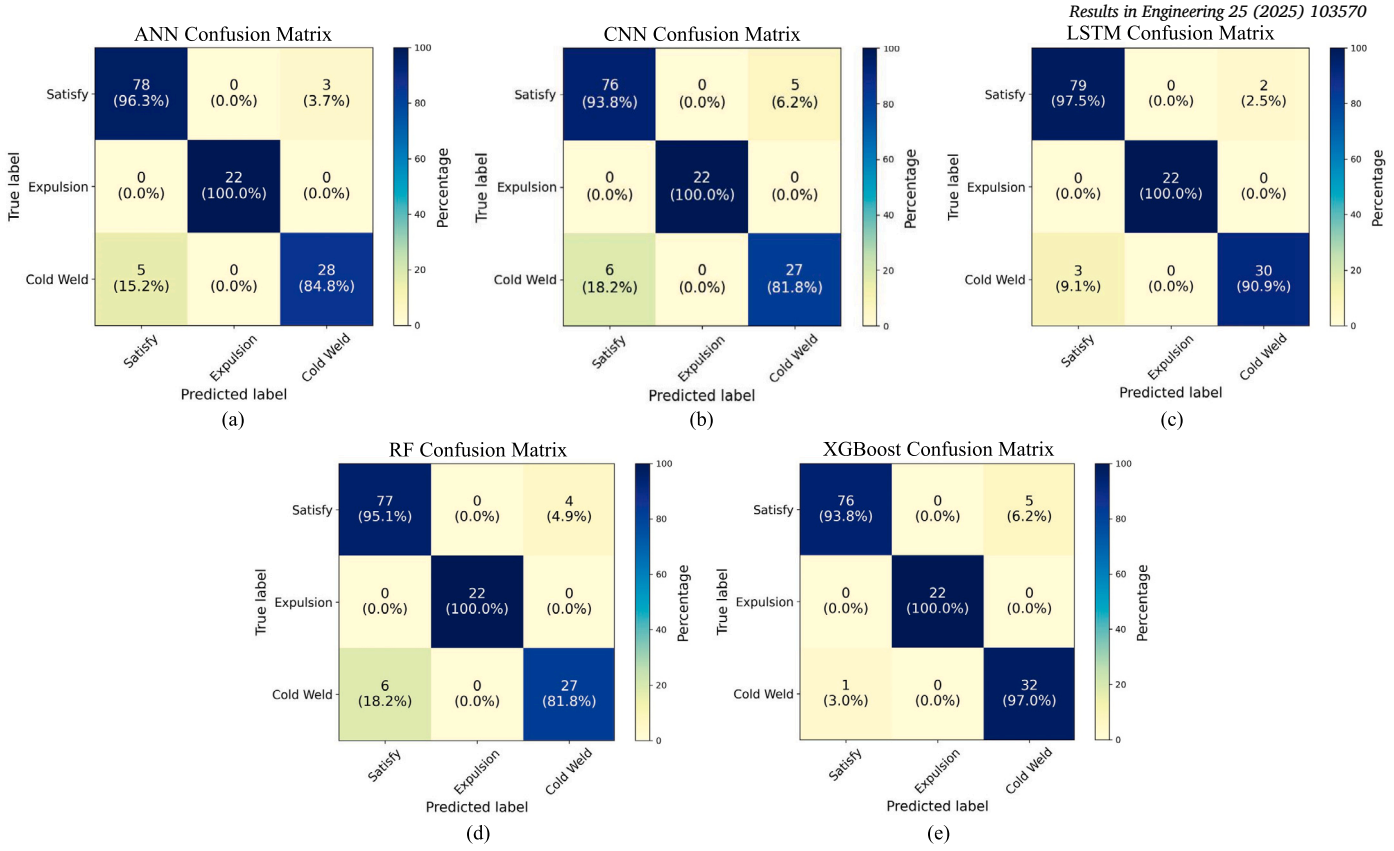


**Fig. 12.** (a) ANN confusion matrix, (b) CNN confusion matrix, (c) LSTM confusion matrix, (d) RF confusion matrix, (e) XGBoost confusion matrix.

the ANN architecture effectively captured general patterns in the data, it lacked the capacity to focus on minority classes, which led to occasional under-killed predictions. This model's limitations underscore the difficulty in using general-purpose neural networks for highly specialized tasks involving imbalanced classes. The CNN, although highly effective in tasks requiring spatial pattern recognition, was less successful here. Since the dataset lacks spatial correlations typical in image or signal data, CNN's convolutional layers could not capture the specific, non-spatial relationships between features essential for weld quality prediction. As a result, CNN struggled with classification accuracy for Cold welds, a limitation inherent to its architecture when applied to non-image-based, tabular datasets.

Similarly, the LSTM network, which is traditionally used for sequential or time-series data, was less effective in this context. The LSTM's temporal dependency modeling did not align with the static nature of weld quality data, which does not follow a sequential pattern. Consequently, the LSTM could not capture the nuanced, inter-feature dependencies required for differentiating weld quality levels, leading to higher error rates in critical classifications.

The RFC showed strong overall performance due to its ensemble approach, which captures feature interactions effectively. However, RFC's reliance on decision tree splits made it challenging to accurately predict less common but essential Cold weld classes. Despite its stability and robust performance for general classification, RFC did not handle the imbalanced class distribution as effectively, resulting in occasional under-killed errors.

XGBoost, on the other hand, achieved the highest accuracy, especially excelling in identifying Cold weld (Level 2) cases with minimal under-killed errors. This model's superior performance can be attributed to several factors. First, XGBoost's iterative boosting process emphasizes misclassified examples, effectively addressing the class imbalance inherent in weld quality data. By focusing computational resources on difficult-to-predict cases through successive iterations, XGBoost significantly reduced errors in edge cases where other models struggled. Additionally, XGBoost's capacity to dynamically capture feature interactions enabled it to identify complex dependencies between welding parameters, which proved crucial for accurate predictions. With an overall accuracy of 95.6% and only one misclassified Cold weld prediction out of 33 unseen samples, XGBoost's robustness makes it an ideal choice for critical quality prediction tasks in manufacturing.

XGBoost's superior results suggest that boosted tree algorithms are well-suited for quality prediction tasks where data is imbalanced and under-killed errors have significant quality implications. Its ability to adjust feature importance dynamically and handle interactions between variables makes it particularly effective for welding datasets where weld quality depends on intricate interdependencies between parameters. Furthermore, XGBoost's built-in regularization mitigates overfitting, an advantage for deployment in real-world production where unseen data might differ from the training set. This robustness underscores its suitability for high-stakes prediction tasks in manufacturing contexts.

The choice of models for this study, including XGBoost, RFC, ANN, CNN, and LSTM, aimed to explore a diverse range of architectures. Models like XGBoost and RFC were selected for their proven effectiveness with structured, tabular data, while ANN offered a flexible, non-linear modeling approach. CNN and LSTM, despite their high performance in image and sequential data tasks, were tested to assess whether their architectures could capture the nuanced feature relationships needed for weld quality prediction. However, as the data did not possess spatial or temporal characteristics, CNN and LSTM faced limitations, highlighting the importance of model alignment with dataset structure.

In summary, XGBoost's capacity to minimize under-killed predictions emphasizes its adaptability and effectiveness in complex prediction tasks involving imbalanced classes. This finding supports the adoption of boosted tree algorithms in scenarios where high-stakes, imbalanced predictions are common, such as weld quality assessments in manufacturing. The results from CNN and LSTM, meanwhile, underline the

**Table 6**
Comparative analysis of XGBoost model before and after F1-score feature elimination.

| No. of Features | Precision | Recall | F1 Score | Train ACC | Test ACC | Unseen ACC | Prediction Time (ms) |
|---|---|---|---|---|---|---|---|
| 29 | 93.333 | 98.148 | 95.344 | 99.543 | 96.364 | 95.588 | 38 |
| 20 | 90.909 | 97.222 | 93.288 | 99.543 | 94.545 | 94.118 | 33 |
| 17 | 96.296 | 99.074 | 97.570 | 99.087 | 98.182 | 97.059 | 33 |
| 15 | 95.118 | 93.600 | 94.696 | 94.545 | 91.176 | 92.314 | 33 |

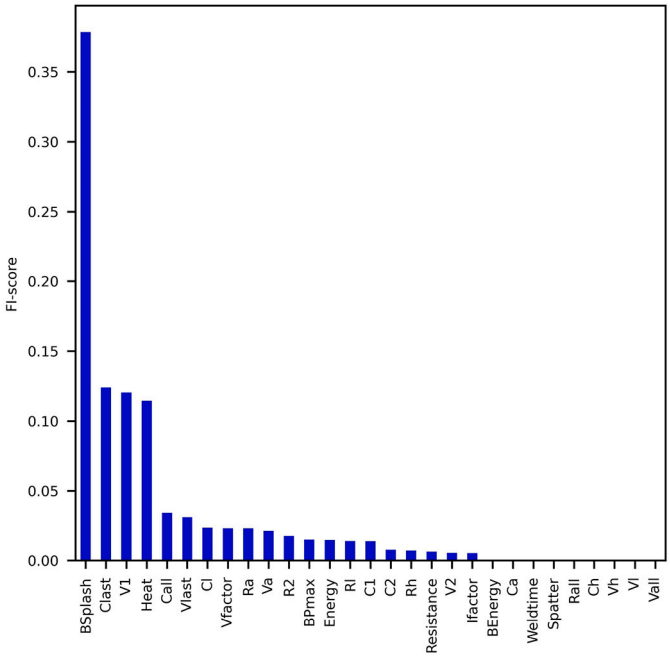


**Fig. 13.** Typical structure of confusion matrix.

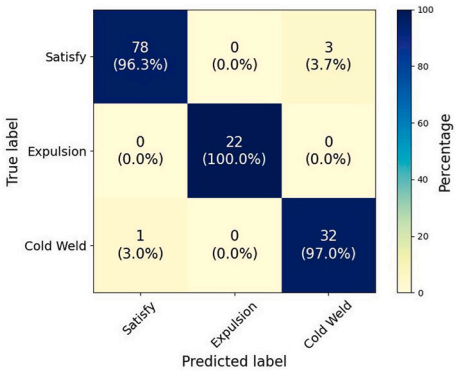


**Fig. 14.** XGBoost confusion matrix after reducing features.

critical need for models that closely match the data's structure. Future work could explore further tailored ensemble methods and feature engineering approaches specific to weld quality to continue enhancing predictive accuracy in this domain.

In our evaluation, the XGBoost model emerged as the optimal choice for deployment in the production process. The processing speed of this model is critical, especially in the automotive manufacturing industry, where efficiency is paramount. According to the company's operational data, each welding point requires a minimum of 5 seconds, including a 2 second interval for the robot to move from one welding point to the next. Specifically, the welding process for the front/rear floor involves almost 90 welding points, necessitating that the entire procedure be completed in around 450 seconds.

To ensure that the model can predict welding quality without causing delays in the production process, it is imperative that it achieves an accuracy rate exceeding 90% and completes predictions within the robot's 2 second movement interval. Currently, the XGBoost model's prediction time stands at 38 milliseconds. However, to provide a buffer for other potential delays, we aim to reduce this processing time further. To this end, we employed the FI-score to identify and eliminate features that contribute minimally to the model's decisions. The FI-score quantifies the relative importance of each feature, with a cumulative total score of 1. We began by removing the feature with the lowest FI-score, proceeding one by one. Fig. 13 shows the impact of feature reduction on the model's performance.

The initial feature set of 31 was reduced in stages: first, a redundant feature was removed, resulting in 29 features; then, features with zero importance scores, as determined by XGBoost, were eliminated, leaving 20 features. Finally, a brute-force approach tested subsets down to 15 features, but retaining 17 features ultimately yielded the best model performance. Table 6 presents a comparative analysis of the XGBoost model's performance and execution time before and after feature reduction. The experiment revealed that reducing the number of features did not always yield optimal results. However, using the reduced FI-score method, the XGBoost model with 17 features achieved the best performance, resulting in a higher accuracy of 97.1% on the unseen dataset, an improvement over the original model. Although this method did not reduce under-killed predictions, it successfully reduced over-killed predictions from 7% to 4%, as shown in Fig. 14. The primary purpose of this feature reduction was to decrease the model's prediction time, and with 17 features, the XGBoost model's prediction time was reduced to 33 milliseconds.

Sensitivity analysis revealed that critical features such as weld current, weld voltage and weld time had the highest impact on predictions, while secondary features such as sheet thickness contributed less significantly. This underscores the importance of accurate sensor data for key parameters in maintaining model performance. Validation techniques, including the use of confusion matrices and testing on unseen production data, demonstrated the robustness and generalizability of the models. The XGBoost model achieved an accuracy of 97.1% on unseen data, confirming its reliability for industrial deployment. Moreover, performance testing under varied conditions, such as sensor noise and reduced feature sets, highlighted the XGBoost model's resilience, maintaining high accuracy even with moderate input variations.

To validate the robustness and applicability of the model in a real-world production setting, we deployed it on the production line from 2023 to 2024. During this period, data from over 100,000 vehicles were captured, with each vehicle involving 8 welding spots monitored by two robots using the machine learning model to predict weld quality in total over 800,000 spot welds in real-time.

The deployment revealed the model's ability to detect cold weld issues with high accuracy. Specifically, 247 vehicles with cold weld defects were identified. These defects would likely have gone unnoticed under traditional random inspection methods, which lack the comprehensive coverage offered by real-time predictive modeling. By identifying these issues early in the process, the model also reduced the likelihood of downstream failures, allowing the production line to address defects proactively and avoid further complications. This demonstrates the effectiveness of the model in enhancing weld quality assurance and reducing production risks.

If we evaluate the potential benefits of applying the model developed in this research to the actual production process, particularly in

welding quality inspection at this company, significant improvements can be expected. Currently, the quality inspection of car body welds using UTs requires 4 operators per shift (2 shifts per day). Implementing machine learning could reduce this number to 2 operators per shift, as the remaining operators would only need to review predictions flagged by the model as Expulsion (Level 1) or Cold weld (Level 2), rather than checking every welding point, including those that are likely to be Satisfy (Level 0).

Moreover, the current method relies on random inspections for Level 0 and Level 2 welds, which may allow some welding errors in the BIW to slip through to the paint section. In contrast, using the prediction model would enable inspection of every car body, as the model predicts welding quality during the process. If a defect is detected, corrective actions can be taken immediately before the RSW robot welds the next point. Rough calculations suggest that reducing the number of operators would lead to considerable cost savings. Additionally, the costs associated with calibrating the UTs could be reduced, as the current process involves 4 UTs.

After the welding process, each car body typically requires 2 operators per shift to inspect for Level 2 defects and polish the surface before painting, particularly to remove any spatter around the welds (Expulsion). However, with the implementation of this real-time weld quality prediction model, maintenance technicians can more effectively adjust the welding current or conditions and clean the body surface at the welding location during the BIW process. This proactive approach reduces the occurrence of expulsions, thereby allowing the number of operators needed for inspection and polishing per shift to be reduced from 2 to 1.

## 5. Conclusion

This study demonstrates the significant potential of various machine learning and deep learning models in accurately predicting the quality of RSW outcomes, categorized as Satisfy (Level 0), Expulsion (Level 1), and Cold Weld (Level 2). The raw data used to build the predictive model was extracted from the WT of the RSW robot. Basic statistical methods were applied, relating pressure, current, and resistance (derived from calculations) to welding time to create the features necessary for the model. Additionally, heat and energy were calculated using parameters from the WT, resulting in a total of 31 features. We confirmed that all features were useful for model building, ensuring that no irrelevant data would influence the machine learning process. This allowed us to eliminate features that were not significantly related to the classification data, reducing the feature set to 29 for model training. We employed different algorithms to compare the results using both default hyperparameters and tuned hyperparameters, including ANN, CNN, LSTM, RF, and XGBoost. Among these, the modified XGBoost model outperformed the others. By evaluating AUC ROC, Train ACC, Test ACC, and confusion matrices—particularly focusing on under-killed predictions as a selection criterion. The XGBoost model achieved a Prediction ACC of 95.6% on unseen data. Further refinement through feature elimination, reducing the feature set to 17, improved prediction speed from 38 milliseconds to 33 milliseconds and increased the model's Prediction ACC to 97.06% while reducing the over-killed rate.

These findings highlight the transformative potential of machine learning techniques in enhancing the quality control of RSW, particularly in real-time production environments. The models' high accuracy suggests a significant opportunity to reduce defects and improve overall manufacturing efficiency and product quality, especially in critical industries like automotive manufacturing. The ability to provide reliable, real-time predictions opens the door for automated quality control systems that can proactively intervene during production, preventing defects and leading to substantial cost savings and operational efficiencies. Future research will aim to refine these models further, improving their predictive accuracy and exploring their integration with other industrial data sources and control systems. This study not only demonstrates the feasibility of advanced machine learning for predicting RSW quality but also paves the way for future innovations that could revolutionize data-driven quality control in manufacturing technology currently used by the factory.

Future advancements in machine learning models will enable AI not only to predict defects but also to diagnose root causes of quality issues, identifying subtle patterns in historical and real-time sensor data to prevent defects before they occur. Self-learning systems will evolve, adapting continuously to changing production conditions and materials, enhancing early detection of quality issues. Additionally, real-time defect detection through edge computing will enable immediate adjustments on the production floor, bypassing cloud latency. Predictive maintenance using digital twins will monitor welding equipment health, predicting wear and malfunctions to reduce downtime and optimize process quality. Future enhancements include incorporating additional parameters like electrode wear, electrode gap, and applied welding force, ensemble learning, hyperparameter tuning, domain adaptation, and model interpretability techniques, as well as integrating predictive models with real-time feedback systems to create a closed-loop quality assurance process. However, there are potential challenges in real-world deployment:

**Scalability and Real-Time Processing:** The XGBoost model outperformed other algorithms due to its ability to handle complex feature interactions and mitigate overfitting, especially with a reduced feature set of 17. Unlike deep learning models such as CNN and LSTM, which require extensive computational resources and large datasets for optimal performance, XGBoost effectively leveraged the structured tabular data and handled noise and missing values efficiently. Its high accuracy and faster inference times (33 ms per prediction) made it particularly well-suited for real-time production environments.

**Dealing with Sensor Noise and Data Quality:** Sensor data in automotive manufacturing environments can be noisy, incomplete, or inconsistent due to equipment malfunctions or environmental factors, potentially degrading model performance. Although XGBoost can handle missing data, excessive noise or data gaps could affect prediction accuracy. To address this, real-time data filtering or additional preprocessing would be essential for improving model robustness.

**Adaptability to Changing Conditions:** Over time, the welding process may vary due to factors like electrode wear or aging equipment. Static models like XGBoost may struggle to adjust without regular retraining. To maintain accuracy, frequent model retraining or an online learning system could be implemented. Techniques like transfer learning could also help the model adapt to changes in production processes or equipment conditions. Addressing these challenges will be crucial for advancing the adoption of machine learning in quality control for RSW, ensuring the models are both accurate and resilient in dynamic production environments.

**Key Contributions:** The study demonstrates the effective application of various machine learning models, particularly XGBoost, for predicting weld quality, improving upon traditional RSW inspection methods. Predictive models provide real-time insights, allowing for continuous monitoring of weld quality, thus reducing the reliance on random post-production inspections and enhancing quality control in real-time. The integration of predictive analytics into the RSW process shows potential for reducing production costs, improving product quality, and increasing efficiency across automotive production lines.

**Future Work:** Future research should focus on integrating IoT-enabled sensors for real-time data collection, providing a constant flow of high-quality data to enhance defect detection accuracy. Developing interpretable machine learning models will help engineers identify factors influencing weld quality and enable informed process adjustments. Moreover, incorporating edge computing architectures will ensure the scalability of predictive models for high-volume production lines, maintaining real-time performance without slowing manufacturing operations. Finally, embedding continuous learning algorithms will allow the mod-

els to adapt to dynamic production conditions, such as electrode wear and material variations, ensuring long-term reliability.

## CRediT authorship contribution statement

Conceptualization, N.C. and J.S.; methodology, N.C. and J.S.; software, N.C.; validation, N.C. and J.S.; formal analysis, N.C. and N.P.; investigation, N.C. and J.S.; resources, N.C. and S.K.; data Creation, N.C. and J.S.; writing-original draft presentation, N.C. and J.S.; writing-review and editing, J.S., N.P. and S.K.; visualization, N.C.; supervision, S.K. and J.S.; project administration, K.C. and J.S.; funding acquisition, K.C. and J.S. All authors have read and agreed to the published version of the manuscript.

## Funding

Not applicable.

## Declaration of competing interest

The authors declare no conflict of interest.

## Data availability

Not applicable.

## References

[1] Jing Wen, Hongde Jia, Real-time monitoring system for resistance spot welding quality, Eng. Res. Express 5 (Jan. 2023), https://doi.org/10.1088/2631-8695/acb130.
[2] Lang Zhou, et al., Comparative study on resistance and displacement based adaptive output tracking control strategies for resistance spot welding, J. Manuf. Process. 63 (Apr. 2020), https://doi.org/10.1016/j.jmapro.2020.03.061.
[3] Dai Wei, et al., Deep learning assisted vision inspection of resistance spot welds, J. Manuf. Process. 62 (Feb. 2021) 262–274, https://doi.org/10.1016/j.jmapro.2020.12.015.
[4] Jian Zhou, et al., Autonomous nondestructive evaluation of resistance spot welded joints, Robot. Comput.-Integr. Manuf. 72 (Dec. 2021) 102183, https://doi.org/10.1016/j.rcim.2021.102183.
[5] Eric Brizes, et al., Evaluation of heat transfer within numerical models of resistance spot welding using high-speed thermography, J. Mater. Process. Technol. 297 (June 2021) 117276, https://doi.org/10.1016/j.jmatprotec.2021.117276.
[6] Zerui Xi, et al., An intelligent inspection method for body-in-white weld quality based on vibration excitation response signals, Measurement 229 (Apr. 2024) 114482, https://doi.org/10.1016/j.measurement.2024.114482.
[7] Arnout Dejans, Oleksandr Kurtov, Patrick Rymenant, Acoustic emission as a tool for prediction of nugget diameter in resistance spot welding, J. Manuf. Process. 62 (Dec. 2020) 7–17, https://doi.org/10.1016/j.jmapro.2020.12.002.
[8] Cameron Summerville, Paul Compston, Matthew Doolan, A comparison of resistance spot weld quality assessment techniques, Proc. Manuf. 29 (Jan. 2019) 305–312, https://doi.org/10.1016/j.promfg.2019.02.142.
[9] Shaik Shafee, B. Naik, Dr Sammaiah, Resistance spot weld quality characteristics improvement by Taguchi method, Mater. Today Proc. 2 (Dec. 2015) 2595–2604, https://doi.org/10.1016/j.matpr.2015.07.215.
[10] Cameron Summerville, et al., Nugget diameter in resistance spot welding: a comparison between a dynamic resistance based approach and ultrasound C-scan, Proc. Eng. 183 (Dec. 2017) 257–263, https://doi.org/10.1016/j.proeng.2017.04.033.
[11] Menachem Kimchi, David Phillips, Resistance Spot Welding Quality, Testing, Monitoring, and Control, ISBN 978-3-031-25782-7, Apr. 2023, pp. 89–104.
[12] Xin-jian Yuan, et al., Resistance spot welding of dissimilar DP600 and DC54D steels, J. Mater. Process. Technol. 239 (Jan. 2017), https://doi.org/10.1016/j.jmatprotec.2016.08.012.
[13] Abhishek Agarwal, et al., Strategic Design Optimization of Cutting Tools for Enhanced Manufacturing Efficiency, ISBN 978-3-031-68270-4, Sept. 2024, pp. 251–276.
[14] Maneerat Rakcheep, et al., Enhancing testing cell set efficiency: a machine learning approach on hard disk drive data, Manuf. Rev. 11 (Apr. 2024) 11, https://doi.org/10.1051/mfreview/2024008.
[15] Prathan Chommuangpuck, Thanasak Wanglomklang, Jiraphon Srisertpol, Fault detection and diagnosis of linear bearing in auto core adhesion mounting machines based on condition monitoring, Syst. Sci. Control Eng. 9 (Jan. 2021) 290–303, https://doi.org/10.1080/21642583.2021.1895901.
[16] Thanasak Wanglomklang, et al., Using fault detection and classification techniques for machine breakdown reduction of the HGA process caused by the slider loss defect, Manuf. Rev. 9 (Aug. 2022), https://doi.org/10.1051/mfreview/2022020.
[17] Chaweng Sapapporn, Soontaree Seangsri, Jiraphon Srisertpol, Classifying and optimizing spiral seed self-servo writer parameters in manufacturing process using artificial intelligence techniques, Systems 11 (May 2023) 268, https://doi.org/10.3390/systems11060268.
[18] I. Polajnar, J. Diaci, Z. Kariž, Overview of resistance spot welding control, Sci. Technol. Weld. Join. 13 (Apr. 2008) 215–224, https://doi.org/10.1179/174329308X283893.
[19] Jaemun Sim, Kyoung-Yun Kim, Hybrid nugget diameter prediction for resistance spot welding, Proc. Manuf. 17 (Jan. 2018) 395–402, https://doi.org/10.1016/j.promfg.2018.10.062.
[20] Xingfang Wang, Kang Zhou, Shanghui Shen, Intelligent parameters measurement of electrical structure of medium frequency DC resistance spot welding system, Measurement 171 (Feb. 2021), https://doi.org/10.1016/j.measurement.2020.108795.
[21] Jiyoung Yu, Adaptive resistance spot welding process that reduces the shunting effect for automotive high-strength steels, Metals 8 (Sept. 2018) 775, https://doi.org/10.3390/met8100775.
[22] Swagat Dwibedi, et al., To investigate the influence of weld time on joint characteristics of Hastelloy X weldments fabricated by RSW process, Mater. Today Proc. 26 (Mar. 2020), https://doi.org/10.1016/j.matpr.2020.02.576.
[23] Hessamoddin Moshayedi, Iradj Sattari-Far, Resistance spot welding and the effects of welding time and current on residual stresses, J. Mater. Process. Technol. 214 (Nov. 2014) 2545–2552, https://doi.org/10.1016/j.jmatprotec.2014.05.008.
[24] Boris Jerman, Samo Simončič, Poor fit-up condition in resistance spot welding, J. Mater. Process. Technol. 230 (Dec. 2015), https://doi.org/10.1016/j.jmatprotec.2015.11.009.
[25] Kang Zhou, Yao Ping, Lilong Cai, Constant current vs. constant power control in AC resistance spot welding, J. Mater. Process. Technol. 223 (Apr. 2015), https://doi.org/10.1016/j.jmatprotec.2015.04.016.
[26] Yu-Jun Xia, et al., Online measurement of weld penetration in robotic resistance spot welding using electrode displacement signals, Measurement 168 (Sept. 2020), https://doi.org/10.1016/j.measurement.2020.108397.
[27] Lilong Cai, Kang Zhou, Tuo Shi, Online measuring the electrical resistivity of molten nugget of stainless steel in resistance spot welding, J. Manuf. Process. 28 (Aug. 2017) 109–115, https://doi.org/10.1016/j.jmapro.2017.05.026.
[28] Yu-Jun Xia, et al., Online quantitative evaluation of expulsion in resistance spot welding, J. Manuf. Process. 46 (Sept. 2019) 34–43, https://doi.org/10.1016/j.jmapro.2019.08.004.
[29] Qasim Nazir, Chenhui Shao, Online tool condition monitoring for ultrasonic metal welding via sensor fusion and machine learning, J. Manuf. Process. 62 (Feb. 2021) 806–816, https://doi.org/10.1016/j.jmapro.2020.12.050.
[30] Jiho Lee, et al., Development of real-time diagnosis framework for angular misalignment of robot spot-welding system based on machine learning, Proc. Manuf. 48 (Jan. 2020) 1009–1019, https://doi.org/10.1016/j.promfg.2020.05.140.
[31] Bassel El-Sari, Max Biegler, Michael Rethmeier, Investigation of the extrapolation capability of an artificial neural network algorithm in combination with process signals in resistance spot welding of advanced high-strength steels, Qual. Assess. Process Manag. Welded Joints (Oct. 2021), https://doi.org/10.20944/preprints202110.0411.v1.
[32] T. Chino, et al., Fast prediction for resistance spot welding deformation using inherent strain method and nugget model, Materials 14 (2021) 1–13, https://doi.org/10.3390/ma14237180.
[33] Lin Hua, et al., In-situ ultrasonic detection of resistance spot welding quality using embedded probe, J. Mater. Process. Technol. 267 (Dec. 2018), https://doi.org/10.1016/j.jmatprotec.2018.12.008.
[34] Kas Ziyad, Manohar Das, An electrothermal model based adaptive control of resistance spot welding process, Intell. Control Autom. 06 (Jan. 2015) 134–146, https://doi.org/10.4236/ica.2015.62014.
[35] P. Ravichandran, et al., Process parameter optimization and performance comparison of AISI 430 and AISI 1018 in resistance spot welding process, Mater. Today Proc. 33 (June 2020), https://doi.org/10.1016/j.matpr.2020.05.197.
[36] Sangun Haa, et al., Estimation of lobe curve with material strength in resistance projection welding, J. Mater. Process. Technol. 263 (2019) 101–111, https://doi.org/10.1016/j.jmatprotec.2018.07.037.